A method for the field assessment of rolling resistance properties of manual wheelchairs

Joseph Bascou[a]*, Christophe Sauret[a], Hélène Pillet[a], Philippe Vaslin[b], Patricia Thoreux[a] and François Lavaste[a,c]

[a]LBM, Arts et Métiers Paristech, 151 Bd de l'Hôpital, Paris 75013, France; [b]3 Clermont Université, Université Blaise Pascal, LIMOS, BP 10448, Clermont-Ferrand 63000, France; [c]CERAH/INI, Antenne de Créteil, 47 rue de l'Echat, Créteil 94000, France

This article presents an examination and validation of a method to measure the field deceleration of a manual wheelchair (MWC) and to calculate the rolling resistances properties of the front and rear wheels. This method was based on the measurements of the MWC deceleration for various load settings from a 3D accelerometer. A mechanical model of MWC deceleration was developed which allowed computing the rolling resistance factors of front and rear wheels on a tested surface. Four deceleration sets were conducted on two paths on the same ground to test the repeatability. Two other deceleration sets were conducted using different load settings to compute the rolling resistance parameters (RPs). The theoretical decelerations of three load settings were computed and compared with the measured decelerations. The results showed good repeatability (variations of measures represented 6–11% of the nominal values) and no statistical difference between the path results. The rolling RPs were computed and their confidence intervals were assessed. For the last three sets, no significant difference was found between the theoretical and measured decelerations. This method can determine the specific rolling resistance properties of the wheels of a MWC, and be employed to establish a catalogue of the rolling resistance properties of wheels on various surfaces.

Keywords: 3D accelerometer; deceleration test; rolling resistance; rolling resistance parameters; wheel; wheelchair

1. Introduction

During manual wheelchair (MWC) locomotion, the user expends energy to generate joint forces and torques, which are transferred to the MWC. The user's mobility thus depends on muscle strength, locomotion techniques, MWC properties (inertial parameters, adjustments, etc.) and substantial sources of energy loss by the MWC, i.e. rolling, turning, bearing and aerodynamic resistances (Cooper 1990; Hofstad and Patterson 1994). In the daily life of MWC users, the ability for straight displacement is considerably important. In this condition, the turning, bearing and aerodynamic resistances can be neglected with regard to rolling resistance (Hofstad and Patterson 1994), which depends on wheels' properties (material, width, radius, etc.), floor type (hardness and roughness) and loads applied on front and rear wheels, for instance. Besides, the rolling resistance was proved to increase when the mass of the loaded MWC is brought forward (de Saint Rémy et al. 2003, de Saint Rémy, 2005; Sauret et al. 2006, 2009, 2010), due to differences in the radii of the front and the rear wheels (Brubaker et al. 1986). Hence, the energy loss by a MWC during propulsion would depend on both the total mass of the MWC-user system and its fore–aft distribution (de Saint Rémy et al. 2003). Thus, characterising the rolling resistance properties of several MWCs should account for these parameters.

Several papers focused on the assessment of MWC rolling resistance using various techniques: several authors measured the global drag force, with a force sensor, sustained by a MWC (loaded with a MWC user or a dummy) rolling on a motor-driven treadmill (Kauzlarich and Thacker 1985; Brubaker et al. 1986; van der Woude et al. 1986; de Groot et al. 2006); others determined the rear wheel deceleration on a roller ergometer (Theisen et al. 1996; Faupin et al. 2004; Kwarciak et al. 2009); or determined the rolling coefficients of front and rear wheels from measurements of a force plate during a deceleration test performed with a MWC loaded with a MWC user (Lemaire et al. 1991). Unfortunately, even if these techniques allowed testing different types of wheels, they did not allow testing different floors. Thus, the results remained confined to the materials of the treadmill belt, the rollers or the force-plate covering. Other techniques, based on deceleration tests (or coast down test) performed in the field, were also described. Coutts (1992, 1994) computed the deceleration of a MWC loaded with a user from a second-order time differentiation of the rear wheels' angular positions (four measurements per turn); others computed the MWC deceleration using the movement differential equations from the time measurement to cross a known distance (Hoffman et al. 2003); or by directly measuring the deceleration from 3D accelerometer with a

MWC loaded by artificial masses (Vaslin and Dabonneville 2000; de Saint Rémy et al. 2003). All these field techniques allowed testing various MWCs equipped with different wheels and on different floors. However, computing deceleration from rear wheels angular displacements (Coutts 1992, 1994) required the use of digital filters before differentiating the data that could alter the deceleration value. In the technique developed by Hoffman et al. (2003), the limit was the assessments of both the initial instantaneous velocity and the actual distances travelled by the MWC achievable with their equipment (photo-electric cells), which did not provide sufficient accuracy. Hence, the technique developed by Vaslin and Dabonneville (2000) would provide better results than the others listed above in quantifying the rolling resistance of various types of wheels and floors.

From another perspective, most methodologies used in the past did not account the influences of both the mass and its fore–aft distribution (Kauzlarich and Thacker 1985; Brubaker et al. 1986; van der Woude et al. 1986; Coutts 1992, 1994; Hoffman et al. 2003). Indeed, few authors distinguished the loads on front and rear wheels (Lemaire et al. 1991; Sauret et al. 2006, 2009). These authors have thus characterised the rolling resistance properties of a MWC by two rolling coefficients (front–rear wheels), which are specific to each wheel–floor couple. In this manner, it was possible to assess the rolling resistance for various masses and fore–aft distributions of this mass.

To characterise the rolling resistance properties of various MWCs on different floors, a good solution could be the measurement of MWC deceleration with a 3D accelerometer during field deceleration tests, then the computing of front and rear wheels' rolling resistance properties, based on the previous works of Vaslin and Dabonneville (2000), de Saint Rémy et al. (2003) and Sauret et al. (2006, 2009). However, before applying this

technique in an extensive way to compare several MWCs or floors, it is important to evaluate the accuracy of the provided results. This study completed the description of the method, provided validation of the repeatability of the tests and assessed the range of potential errors.

2. Materials and methods

2.1 Modelling of rolling resistance

The MWC, loaded with a fixed mass and decelerating on a straightforward motion under the only action of the rolling resistance – neglecting bearing, slipping and air resistances (Hofstad and Patterson 1994; Van der Woude et al. 2006) – was modelled as presented in Figure 1. The mechanical model that links the deceleration of the global center of mass (COM) (γ_G) to both forces and torques exerted on the system (MWC + artificial masses) is detailed in Appendix A and is written as follows (see symbols description in Table 1):

$$\gamma_G = -mg \frac{\left(\frac{\lambda_f}{r_f}\frac{d_r}{w_b} + \frac{\lambda_r}{r_r}\frac{d_f}{w_b} + \frac{\lambda_f\lambda_r}{r_fr_r}\frac{r_f-r_r}{w_b}\right)}{\left(m + \frac{I_f}{r_f^2} + \frac{I_r}{r_r^2}\right)\left(1 + \frac{\lambda_f-\lambda_r}{w_b}\right) + \left(m + \frac{I_f}{r_fh} + \frac{I_r}{r_rh}\right)\left(\frac{\lambda_r}{r_r} - \frac{\lambda_f}{r_f}\right)\frac{h}{w_b}}.$$

(1)

This equation is an exhaustive model of rolling resistance. However, it can be correctly approximated ($<3\%$ error) by the following expression, leaving out the negligible terms (see details in Appendix B):

$$\gamma_G = -g\left(\frac{\lambda_f}{r_f}\frac{d_r}{w_b} + \frac{\lambda_r}{r_r}\frac{d_f}{w_b}\right).$$

(2)

In this expression, λ_f and λ_r are the rolling resistance parameters (RPs) of the front and rear wheels, respectively. They represent the fore–aft distance between the theoretical centre of rotation of the wheel on the floor
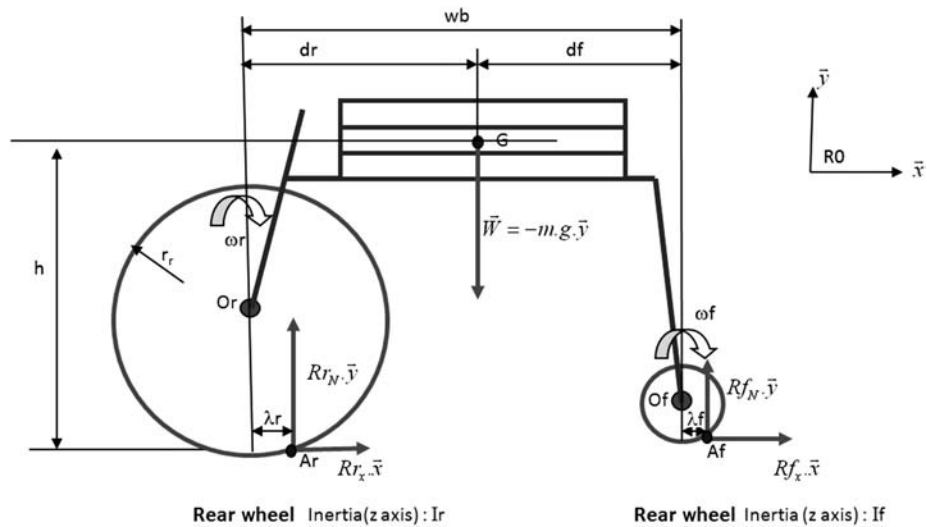

Figure 1.   Free body diagram of rolling resistance.

Table 1. Symbols description.

Symbol	Description	Unit
γ_G	Deceleration of the global COM	$m\,s^{-2}$
g	Gravity acceleration	$m\,s^{-2}$
m	Total mass	kg
λ_f	Rolling RP of the front casters	m
λ_r	Rolling RP of the rear wheels	m
r_f	Radius of the front casters	m
r_r	Radius of the rear wheels	m
d_f	Fore–aft distance between global COM and front wheels centre	m
d_r	Fore–aft distance between global COM and rear wheels centre	m
w_b	Wheelbase (fore–aft distance between front and rear wheels centres)	m
h	Height of the global COM with respect to the ground	m
I_f	Moment of inertia of the two front casters along their rotational axles	$kg\,m^2$
I_r	Moment of inertia of the two rear wheels along their rotational axles	$kg\,m^2$
W_f	Weight applied on front casters	N
W_r	Weight applied on the rear wheels	N
m_f	Mass applied on the front wheels	kg
m_r	Mass applied on the rear wheels	kg
F_{roll}	MWC rolling resistance	N

(normal projection of wheel centre on the floor) and the centre of pressure in the contact area where the resulting ground reaction force is applied. As a consequence, the ground reaction force creates a resisting moment with respect to the theoretical centre of rotation on the floor, namely the moment of rolling resistance. The distances λ_f and λ_r are a consequence of the material inelastic properties of both wheels and floor (i.e. hysteresis phenomenon) and characterise the contact between the wheel and the ground.

The ratio between the rolling RP (λ) and the wheel radius (r) is called the rolling resistance factor and represents the effective rolling resistance property of a wheel. Then, the rolling resistance factor characterises the wheel.

Finally, the resultant force of rolling resistance (F_{roll}), characterising the MWC, can be obtained by multiplying Equation (2) by the total mass (m) to give a formulation that is consistent with those already expressed (Cooper 1990; Sauret et al. 2009):

$$F_{roll} = m\gamma_G = -\left(\frac{\lambda_f}{r_f}W_f + \frac{\lambda_r}{r_r}W_r\right). \qquad (3)$$

Furthermore, Equation (2) can also be written using the mass proportion on the front and rear wheels:

$$\gamma_G = -g^*\left(\frac{\lambda_f}{r_f}P_f + \frac{\lambda_r}{r_r}P_r\right). \qquad (4)$$

2.2 Experimental protocol

To reproduce the hypothesis leading to Equation (4) for a given MWC and floor, the selected MWC was loaded concatenating additional masses on the seat and close to the floor. This way, the MWC oscillations in horizontal and sagittal plane, due to the frame deformation and the pushing of the MWC, were limited. Its deceleration during free-wheeling phase was then measured.

The estimation of the rolling resistance factors in Equation (4) required the measurement of the other values. The resulting loads on front wheels and on rear wheels were measured with a specific large weight-scale platform (resolution: 0.05 kg). A gravitational acceleration value of 9.81 m/s^2 was used. The wheel radii were measured with a calliper rule. The deceleration value during the free-wheeling phase associated with this load repartition was obtained by conducting various deceleration tests (see below) and data processing.

2.2.1 Deceleration tests

The deceleration test provided a deceleration value for the free-wheeling phase, and consisted in pushing the MWC and allowing it to decelerate along a straight corridor, measuring the deceleration during this time.

During the acquisition, various phases have to be observed (1) static phase: lasts for 2 s and is used for data processing; (2) push phase: the MWC is manually pushed to 1–3 km/h; (3) free deceleration phase; (4) stop phase: as the deceleration length was limited, the MWC was manually stopped after a 4-m long deceleration phase and (5) static phase: used for data processing.

The deceleration value was measured during the free deceleration phase (phase 3) using a wireless 3D accelerometer (Beanscape AX-3D, Beanair, Neuville-sur-Oise, France, sensitivity: $\pm 2\,g$) fixed on the additional masses (a thin foam was used to limit the sensor vibrations) and at a 100 Hz frequency (Vaslin and Dabonneville 2000). Caution was taken to align the accelerometer x-axis with the travel direction (see x-axis of the reference frame in Figure 2).

The start and stop positions and the trajectory as well as the angular start position of the rear wheels (valves down) were controlled; the test was conducted in a narrow lane of 60-cm width drawn on the floor and was rejected if the MWC deviated from this lane (Example : lane A in Figure 3).

2.2.2 There-and-back deceleration

To overcome the limit due to the unevenness of the ground, a there-and-back procedure was adopted: for each deceleration test in one way, another deceleration test was conducted on the way back (Coutts 1991, 1994; Sauret et al. 2010), keeping the same deceleration path. Hence,
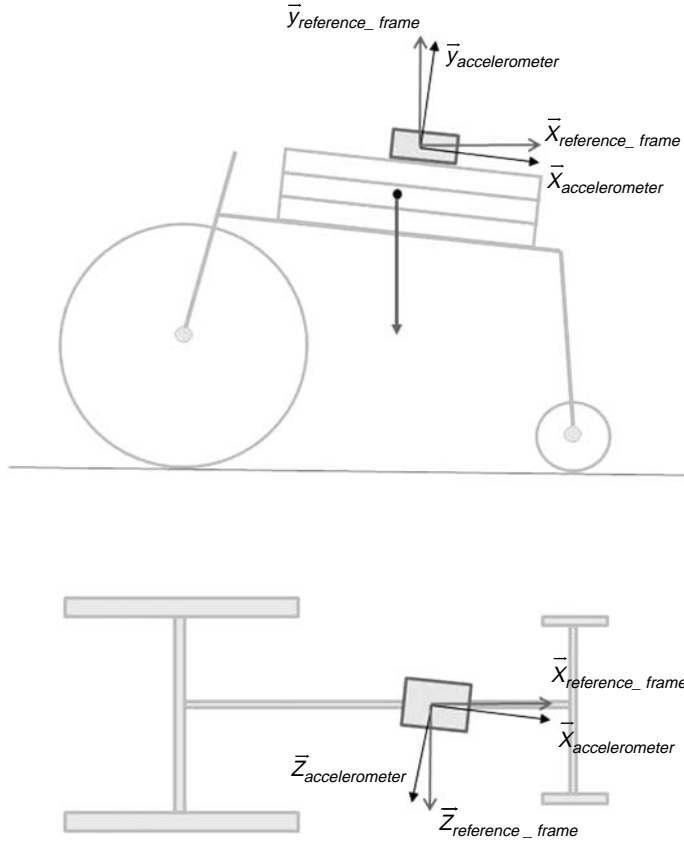
Figure 2.   Accelerometer axis and reference frame.

the tests were always paired, with half of the tests made in one direction and the other half on the reverse direction, providing one deceleration value for each pair.

2.2.3   Sets deceleration for each load repartition

A set of there-and-back decelerations allowed defining the deceleration value associated with Equation (4) to a given

Figure 3.   Corridor description for validation tests.

load distribution. Within a set, the load repartition remained constant (the position of the additional mass did not vary) and the MWC deceleration was evaluated by conducting various there-and-back tests on a horizontal floor. In our study, 10 there-and-back procedures were performed for each set, providing 10 deceleration values. One set was done for every load distribution presented in Table 2.

2.3   Data processing: deceleration and rolling resistance properties computation

2.3.1   Deceleration test processing

When the *x*-axis of the 3D accelerometer was perfectly aligned with the travel direction, a 1D accelerometer was sufficient. Unfortunately, it is impossible to perfectly align manually the *x*-axis with the travel direction both in the sagittal and in the horizontal planes (Figure 2). As the errors due to small misalignments in the horizontal plane could be neglected, those caused by misalignments in the sagittal plane (Figure 2) could induce large errors on MWC deceleration measure, due to the action of the gravitational acceleration.

Therefore, to correct misalignments that occurred during the deceleration test, various steps of signal processing were applied to the raw data:
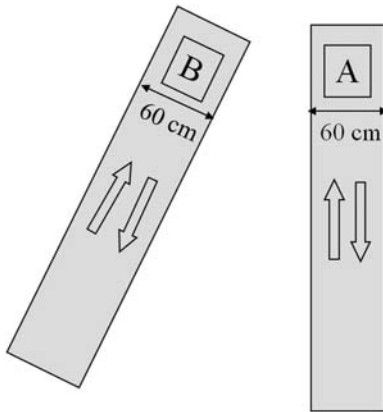
Table 2. Deceleration results for deceleration sets conducted with various corridors, total load and load distribution.

Set number	No of valid there-and-back procedures	Total mass (kg)	Total load on front wheels (%)	Corridor	Outward deceleration ($\pm$ SD) ($\times 10^{-2}$ m/s^2)	Forward deceleration ($\pm$ SD) ($\times 10^{-2}$ m/s^2)	Set deceleration ($\pm$ SD) ($\times 10^{-2}$ m/s^2)	Set deceleration confidence interval ($\times 10^{-2}$ m/s^2)
S_1	9	75.10	29	A	4.2 ($\pm$0.8)	5.4 ($\pm$0.7)	4.8 ($\pm$0.3)	0.4
S_{1B}	10	75.10	29	B	4.3 ($\pm$0.6)	4.8 ($\pm$0.5)	4.5 ($\pm$0.4)	0.5
S_2	10	75.10	64	A	6.4 ($\pm$0.6)	7.0 ($\pm$0.6)	6.7 ($\pm$0.4)	0.4
S_{2B}	9	75.10	64	B	6.2 ($\pm$0.5)	7.4 ($\pm$0.4)	6.8 ($\pm$0.3)	0.4
S_3	10	99.10	22	A	3.7 ($\pm$0.5)	4.4 ($\pm$0.4)	4.0 ($\pm$0.2)	0.3
S_4	10	90.10	69	A	7.5 ($\pm$0.5)	7.8 ($\pm$0.4)	7.6 ($\pm$0.3)	0.4
S_5	10	75.10	50	A	5.4 ($\pm$0.6)	5.4 ($\pm$0.5)	5.4 ($\pm$0.3)	0.4
S_6	10	58.15	37	A	4.3 ($\pm$0.6)	5.0 ($\pm$0.5)	4.6 ($\pm$0.3)	0.4
S_7	10	58.60	51	A	5.2 ($\pm$0.5)	6.4 ($\pm$0.6)	5.8 ($\pm$0.3)	0.3

- First step. A rotation matrix was defined to transform the accelerometer frame (R_{acc}) to the measurement frame ($R_{measure}$) and was defined as follows: the gravity measurement during the first static phase (1st part) defined the vertical $y_{measure}$-axis (Vaslin and Dabonneville 2000; de Saint Rémy et al. 2003); the transversal $z_{measure}$-axis was the same as the transversal z_{acc}-axis; the $x_{measure}$-axis, pointing in the travel direction, was defined by the cross product of $y_{measure}$ by $z_{measure}$. This axis was perfectly horizontal at the beginning of the measure and was the one used to measure the MWC deceleration. The raw acceleration vector was then transformed using the rotation matrix into the measure vector. The components of this vector were the deceleration value along $x_{measure}$-axis, the gravity acceleration along $y_{measure}$-axis and the MWC transversal oscillations along $z_{measure}$-axis (equal to zero in theory).
- Second step. The horizontal velocity was calculated by a first-order time integration of the fore–aft deceleration (along $x_{measure}$-axis) from the start of the push phase (2nd part) to the complete stop of the MWC (beginning of the 5th part). A constant value was subtracted to the $x_{measure}$-data to obtain a null velocity at the end of the movement (see Figure 4). This correction corrects small misalignments of the $x_{measure}$-axis with the deceleration vector, which otherwise induce a drift in the measured velocity.
- Third step. The deceleration phase was manually identified from maximal velocity (end of the push phase) until the beginning of the stop phase (characterised by a break in the velocity decrease). The mean deceleration value (along $x_{measure}$-axis) during the deceleration phase was then calculated. This deceleration value was considered as the MWC centre of mass deceleration during the free deceleration phase of the test.

2.3.2 There-and-back set processing

To obtain the deceleration value for each there-and-back procedure, the two decelerations obtained for the pair of deceleration tests were averaged, which allowed cancelling out the tiny slope effect that always exists even on an apparently flat ground.

Prior to computing the mean deceleration value of each set (composed of 10 there-and-back deceleration values), the outliers identified using the Box and Whiskers Plots method (Le Guen 2001) were rejected.

2.3.3 Wheel rolling resistance factors computation

From the simplified Equation (4), knowing the wheel radius, the load distribution and the MWC COM
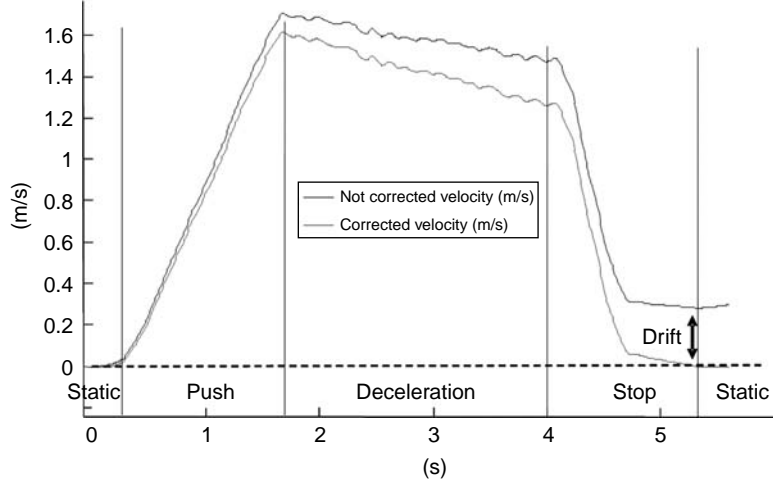
Figure 4.   Initial and corrected velocity profile during the deceleration.

deceleration for various load conditions, a set of equations could be formulated, in which only the rolling RPs λ_f and λ_r are the unknown variables, and were assumed to be unchanged when the loads on each wheel varied.

The set of equations to be solved was presented in the following system:

$$\frac{\lambda_r}{r_r}P_{fi} + \frac{\lambda_r}{r_r}P_{ri} = \frac{\gamma_i}{-g}, \tag{5}$$

where the indices i represented the equation set number.

This system of Equations (5) could be expressed in a matrix form:

$$\underbrace{\begin{bmatrix} P_{f1} & P_r \\ P_{f2} & P_{r2} \\ \cdots & \cdots \end{bmatrix}}_{\text{distribution matrix } (n\times2)} \underbrace{\begin{bmatrix} \lambda_f/r_f \\ \lambda_r/r_r \end{bmatrix}}_{\text{matrix of unknown } (2\times1)}$$

$$= -1/g. \underbrace{\begin{bmatrix} -\gamma_{G1} \\ -\gamma_{G2} \\ \cdots \end{bmatrix}}_{\text{acceleration matrix } (n\times2)}. \tag{6}$$

Here, the wheel radii were known, but were integrated in the unknown matrix to maintain a simple equation system. The unknown elements were then the rolling resistance *factors*.

More generally, the system could then be expressed by

$$[M_D] \cdot [M_{RF}] = \frac{-1}{g} \cdot [M_\gamma], \tag{7}$$

where M_D is the distribution matrix, M_{RF} is the matrix of unknowns and M_γ is the acceleration matrix.

This can be solved by the following equation, provided that the determinant of $([M_D]^T[M_D])$ is not null, then the matrix invertible is

$$[M_{RF}] = \frac{-1}{g} \cdot ([M_D]^T \cdot [M_D])^{-1} \cdot [M_D]^T \cdot [M_\gamma]. \tag{8}$$

In reality, as the measurements suffer from approximations, the $([M_D]^T[M_D])$ matrix has to be well conditioned, which means that the resulting unknown matrix computation need not change significantly when a random perturbation is placed in the distribution or in the acceleration matrix (Cabane 1998). As two unknowns are present in the system, at least two sets of equations are necessary to solve the system, which means two load conditions and two deceleration values. If more load conditions are considered, the system will be overabundant and the results will be averaged: solved through a root mean square regression, the system becomes less sensitive to small errors when the number of points rises.

2.3.4   Wheel rolling RPs

The rolling RPs could be calculated by multiplying the rolling resistance factors of the front and rear wheels by their respective radii. The values of the rolling resistance factors and the rolling RPs were considered independent of the load applied on each wheel.

2.3.5   Confidence interval on decelerations

The normal distribution of the deceleration values within a set was checked with the Shapiro–Wilk test ($p = 0.05$) and the 95% confidence interval was finally calculated using the Student law (Rakotomalala 2008), which allows

the estimation of the accuracy of the deceleration value obtained for each set.

To quantify the impact of this accuracy on rolling RPs, a Monte Carlo simulation was performed (Kalos and Whitlock 1986). To proceed, the system expressed in Equation (8) was solved 10,000 times introducing a white noise on decelerations, which varied within their confidence interval (Bascou et al. 2010). The accuracy of the front and rear wheels' rolling RPs was then estimated from the standard deviation provided by the 10,000 computations.

2.4 Validation

2.4.1 Experimental procedure for method validation

The validation of the method was performed using various sets of 10 there-and-back decelerations, conducted on a hard and smooth surface (polished concrete ground) with one MWC (Kushall Champion carbone, Invacare, Elyria, Ohio, USA, in its sale configuration), in which the rear wheels were inflated up to 6 bars (87 psi). The wheel radii were 29 cm for rear wheels and 6 cm for front wheels. For each set, the additional masses and/or their distribution varied. Two 6-m-long and 60-cm-wide corridors, drawn on the same ground (see Figure 3), were used to perform the deceleration tests and sets and were named 'corridor A' and 'corridor B'.

2.4.2 Measurement validation: influence of the path on the deceleration results

To assess the influence of the path choice on this method, two deceleration sets were conducted using one load distribution on corridors A and B (set numbers S_1 and S_{B1} in Table 2). Then the load conditions were changed and two other sets were conducted on corridors A and B as presented in Table 2 (set numbers S_2 and S_{B2}). For each set, the normality of the there-and-back decelerations was checked, then Student t-tests were used to compare sets S_1 with S_{B1} and sets S_2 with S_{B2}.

2.4.3 Model validation

Two more sets were performed on corridor A (S_3 and S_4, Table 2) and their mean decelerations were used, with S_1 and S_2 mean decelerations, to compute the rolling resistance factors of the front and rear wheels. Three additional sets (S_5, S_6 and S_7, Table 2) were also performed on corridor A and were used for validation by comparing the decelerations measured to the decelerations assessed from the rolling resistance factors previously obtained (from S_1, S_2, S_3 and S_4).

2.5 Results

The results of sets S_1, S_{B1}, S_2 and S_{B2} are described in Table 2. Two outliers were rejected for sets S_1 and S_{B2}.

For three of the four load conditions (sets S_1, S_2 and S_{B2}), significant differences were found between deceleration tests conducted in the reverse directions. These differences ranged from 0.006 (S_{1B}) to 0.012 m s^{-2} (S_1 and S_{2B}), and in the Student t-test from 2.2 to 5.74.

Considering the there-and-back decelerations (gathering outward and forward deceleration tests), the set decelerations ranged from 0.045 to 0.068 m s^{-2} for S_{1B} and S_{2B}, respectively. The intra-set variability, expressed through the standard deviation, ranged from 0.003 (S_1 and S_{2B}) to 0.004 m s^{-2} (S_{1B} and S_2). Considering the 95% confidence interval, the measurement uncertainty on deceleration ranged from ± 0.004 to ± 0.005 m s^{-2}, which was 6–11% of the nominal value. Comparing corridor A with corridor B, the mean decelerations differed by 0.003 m s^{-2} (between S_1 and S_{1B}) and 0.001 m s^{-2} (between S_2 and S_{2B}); however, these differences were insignificant (Student t-test = 1.42 and 0.49, respectively).

The results of sets S_3 and S_4 are presented in Table 2. The computation of rolling resistance factors using sets S_1, S_2, S_3 and S_4 decelerations provided the rolling resistance factors and the Monte Carlo simulation provided an estimation of the confidence intervals: $\lambda_{\text{front}}/r_{\text{front}}$ (± 2SD) $= 9.8 \times 10^{-3}$ ($\pm 1.1 \times 10^{-3}$) and $\lambda_{\text{rear}}/r_{\text{rear}}$ (± 2SD) $= 2.6 \times 10^{-3}$ ($\pm 0.8 \times 10^{-3}$). The rolling RPs could then be calculated: λ_{front} (± 2SD) $= 0.6 \times 10^{-3}$ m ($\pm 0.03 \times 10^{-3}$) and λ_{rear} (± 2SD) $= 0.8 \times 10^{-3}$ m ($\pm 0.1 \times 10^{-3}$).

The rolling resistance factors and the load conditions of sets S_5, S_6 and S_7 were used to predict their decelerations: 0.061 m s^{-2} (± 0.009) for set S_5, 0.052 m s^{-2} (± 0.009) for set S_6 and 0.062 m s^{-2} (± 0.009) for set S_7. The differences between the computed and the measured decelerations for S_5, S_6 and S_7 were 0.007, 0.006 and 0.004 m s^{-2}, respectively, which were lower than the confidence intervals of each set deceleration.

Multiplying the deceleration values obtained for each set by the total masses yielded drag forces ranging between 2.7 N (58 kg, 37% on the front wheels) and 6.9 N (90.8 kg, 69% on the front wheels).

3. Discussion

Owing to the proposed method, the MWC decelerations could be obtained for various sets of load conditions and were consistent with previous studies (Coutts 1991; de Saint Rémy 2003; Sauret et al. 2009). The study underlined the significant influence of the load distribution on the deceleration: for example a 52% increase in the deceleration was observed when the load repartition varied

from 29% (S_1) to 64% (S_2), although the total mass remained the same. These results were expected and consistent with previous results obtained by de Saint Rémy et al. (2003) and Sauret et al. (2009, 2010).

The results also showed a good repeatability in the deceleration tests when performed in the same direction, but showed differences between tests in one way and tests in the way back. This underlines the significant influence of small floor deformations on the measured deceleration and the need for there-and-back procedures, with which the method proved to be sufficiently robust to conduct experiments on different paths on the same ground without altering the results (providing the ground properties are the same, as shown by the comparison of the sets S_1, S_{1B}, S_2 and S_{2B} for different corridors). This novel result allows the comparison of wheel properties of a MWC on various grounds (concrete, carpet, etc.), ensuring that differences in deceleration values are directly correlated with the ground material properties, rather than its deformities.

To the authors' knowledge, the rolling resistance factors and parameters of the front and rear wheels of MWC were calculated only once before (Sauret et al. 2006, 2009): the rolling resistances found in our study were lower, but this could be explained by differences in the wheel and ground types (concrete ground vs. athletic track ground). The calculation of predicted decelerations for sets S_5, S_6 and S_7 and their comparison with the measured deceleration showed the validity of the proposed model. The rolling resistance factors were significantly higher on the front wheels than on the rear wheels for the tested MWC, which is consistent with the increase in rolling resistance with the front wheels distribution of the total mass. This could be explained by the mechanical model of rolling resistance: the front wheels' radii were five times smaller than the rear wheels' radii and their rolling RPs were quite the same (0.6×10^{-3} m vs. 0.8×10^{-3} m). Therefore, the front wheel rolling resistance factor, which is the ratio of the rolling RP to the radius of the front wheel, was four times smaller than that of the rear wheel one. Taking into account the confidence intervals, the front and rear rolling resistance *factors* could be distinguished: the two standard deviations on the rolling RPs were 6% of the nominal value for the front wheels and 15% for the rear wheels, which must be taken into account when comparing the two wheels on the same ground or two grounds for the same wheels.

The rolling drag forces were in accordance with those found by Coutts (1992, 1994) and Brubaker et al. (1986). However, the use of the drag force to compare the wheelchairs must be handled with extreme caution, as it mainly depends on the load distribution (de Saint Rémy et al. 2003).

4. Conclusion

This study completed the work of previous researches on the deceleration method (Coutts 1991; de Saint Rémy et al. 2003; Sauret et al. 2006, 2009), and proved the interest and the reliability of this technique in assessing the effect of the ground and front and rear wheel choice on the MWC deceleration and rolling drag force.

The mechanical model allowed the front and rear wheels rolling resistance *factors* and *parameters* to be computed with an acceptable accuracy. The use of this method could allow the creation of a database of the rolling resistance properties of various wheels on different surfaces: the rolling drag force of a wheelchair could then be calculated from the front and rear wheel types, the ground type and the load distribution. This database would allow a comparison between MWC on a defined floor, according to the load distribution and from an energetic point of view.

References

Bascou J, Sauret C, Pillet H, Lavaste F, Vaslin P. 2010. Error estimations of wheelchair deceleration tests using a 3-D accelerometer. Comput Methods Biomech Biomed Eng. 13(suppl. 4):21–22.

Brubaker CE, McLaurin CA, McClay IS. 1986. Effects of side slope on wheelchair performance. J Rehabil Res Dev. 23(2): 55–58.

Cabane R. 1998. Méthodes numériques en algèbre linéaire. Techniques de l'ingénieur, sciences fondamentales, mathématiques pour l'ingénieur, methodes numeriques, algèbre linéaire et optimisation méthodes numériques en algèbre linéaire, traitement des erreurs en algèbre linéaire. Techniques de l'ingénieur, Référence AF485.

Cabelguen J-C. 2008 Développement d'outils pour l'analyse et la quantification des interactions utilisateur-fauteuil-environnement lors de déplacements en fauteuil roulant manuel. Doctorat Biomécanique, Laboratoire de BioMécanique, Paristech > ENSAM 2008ENAM0048. p.144.

Cooper RA. 1990. A system approach to the modeling of racing wheelchair propulsion. J Rehabil Res Dev. 27(2): 151–162.

Coutts KD. 1991. Dynamic characteristics of a sport wheelchair. J Rehabil Res Dev. 28(3):45–50.

Coutts KD. 1992. Dynamics of basketball. Med Sci Sports Exerc. 24(2):231–234.

Coutts KD. 1994. Drag and sprint performance of wheelchair basketball players. J Rehabil Res Dev. 31(2):138–143.

de Groot S, Zuidgeest M, van der Woude L. 2006. Standardization of measuring power output during wheelchair propulsion on a treadmill: pitfalls in a multi-center study. Med Eng Phys. 28:604–612.

de Saint Rémy N. 2005. Modelisation and determination of biomechanical parameters of manual wheelchair locomotion. PhD Thesis. Blaise Pascal university, Clermont-Ferrand, France (in French).

de Saint Rémy N, Vaslin P, Dabonneville M, Martel L, Gavand A. 2003. Dynamique de la locomotion en fauteuil roulant manuel: influences de la masse totale et de sa répartition antéropostérieure sur la résultante des forces de freinage. Sci Sports. 18(3):141–149.

Faupin A, Campillo P, Weissland T, Gorce P, Thevenon A. 2004. The effects of rear-wheel camber on the mechanical parameters produced during the wheelchair sprinting of handibasketball athletes. J Rehabil Res Dev. 41(3B): 421–428.

Hoffman MD, Millet GY, Hoch AZ, Candau RB. 2003. Assessment of wheelchair drag resistance using a coasting deceleration technique. Am J Phys Med Rehabil. 82(11): 880–889.

Hofstad M, Patterson PE. 1994. Modelling the propulsion characteristics of a standard wheelchair. J Rehabil Res Dev. 31(2):129–137.

Kalos M, Whitlock P. 1986. Monte Carlo methods. New York, NY: John Wiley and Sons.

Kauzlarich JJ, Thacker JG. 1985. Wheelchair tire rolling resistance and fatigue. J Rehab Res Dev. 22(3):25–41.

Kwarciak AM, Yarossi M, Ramanujam A, Dyson-Hudson TA, Sisto SA. 2009. Evaluation of wheelchair tire rolling resistance using dynamometer-based coast-down tests. J Rehabil Res Dev. 46(7):931–938.

Le Guen M. 2001. La boîte à moustaches de TUKEY un outil pour initier à la Statistique. Statistiquement vôtre. 4.

Lemaire ED, Lamontagne M, Barclay HW, John T, Martel G. 1991. A technique for the determination of center of gravity and rolling resistance for tilt-seat wheelchair. J Rehabil Res Dev. 28:51–58.

Rakotomalala R. 2008. Tests de normalité: Techniques empiriques et tests statistiques. Support de cours Université Lumière Lyon. 2.

Sauret C, de Saint Rémy N, Vaslin P, Cid M, Dabonneville M, Kauffmann P. 2006. Theoretical comparison of the resultant braking force applied on a manual wheelchair within a propulsion cycle on the field and on laboratory ergometers. ASME J Model Measure Cont Ser C. 67(suppl. Handicap 2006):43–52.

Sauret C, Vaslin P, Dabonneville M, Cid M. 2009. Drag force mechanical power during an actual propulsion cycle on a manual wheelchair. IRBM. 30(1):3–9.

Sauret C, Bascou J, Pillet H, Lavaste F, Vaslin P. 2010. Repeatability of wheelchair deceleration tests using a 3-D accelerometer. Comput Methods Biomech Biomed Eng. 13(suppl. 4):137–138.

Sauret C. 2010. Kinetics and energetics of manual wheelchair propulsion. PhD Thesis. Blaise Pascal university, Clermont-Ferrand, France (in French).

Theisen D, Francaux M, Fayt A, Sturbois X. 1996. A new procedure to determine external power output during handrim wheelchair propulsion on a roller ergometer: a reliability study. Int J Sports Med. 17:564–571.

Van der Woude LHV, de Groot G, Hollander AP, van Ingen Schenau GJ, Rozendal RH. 1986. Wheelchair ergonomics and physiological testing of prototypes. Ergonomics. 29:1561–1573.

Van der Woude L, de Groot S, Janssen T. 2006. Manual wheelchairs: research and innovation in sports and daily life. Sci Sports. 21:226–235.

Vaslin P, Dabonneville M. 2000. Use of a 3D accelerometer for kinetic analysis of wheelchair propulsion. Proceedings of XIIth Conference of the European Society of Biomechanics, 28–33 August, Dublin (Ireland). p. 345.

Appendix A

This appendix aims to develop the mechanical model providing Equation (1) carrying on the COM deceleration of the loaded MWC during the deceleration phase of a coast down test and is based on Figure 1: the sagittal plane is considered and the front and rear wheels are treated as pairs.

At first, considering the loaded MWC (frame + wheels) during this phase, the exterior forces applied are the total weight ($\vec{W}$) and the ground reaction forces on the front ($\vec{R}_f$) and rear wheels ($\vec{R}_r$); applying the second law of Newton on the system equation along the fore-and-aft and the vertical directions gives

$$\sum F_{x,\text{ext}\to\text{WMC}} = m\gamma_G \Leftrightarrow R_{fx} + R_{rx} = m\gamma_G, \qquad (A1)$$

$$W + R_{fN} + R_{rN} = 0, \qquad (A2)$$

where R_{fx} and R_{rx} are the fore-and-aft components of the ground reaction forces applied on the front and rear wheels, respectively; R_{fN} and R_{rN} are the normal components, m is the total mass and γ_G is the fore-and-aft COM deceleration of the loaded MWC.

Considering the front wheels and their centre O_f, the equality of the torque of the exterior forces in O_f with the angular momentum variation in O_f, projected on z-axis, gives

$$\sum M_{z,\text{ext}\to\text{front wheels}} = I_{z,\text{front wheels}} \times \Gamma_z = I_f \times \Gamma_z,$$

where I_f is the front wheel inertia along z-axis and $\Gamma_z = \gamma_G/r_f$ is the wheel angular acceleration.

The torque of exterior forces can be expressed by

$$\sum M_{z,\text{ext}\to\text{front wheels}}$$

$$= M_{z,O_f,\text{frame}\to\text{front wheels}} + M_{z,O_f,\text{ground}\to\text{front wheels}}$$

$$= 0 + M_{z,A_f,\text{ground}\to\text{front wheels}} + (O_fA_f \wedge F_{\text{ground}\to\text{front wheels}}) \cdot z$$

$$= 0 + 0 + (-r_f \cdot y + \lambda \cdot x) \wedge (R_{fN} \cdot y + R_{fx} \cdot x) \cdot z$$

$$= r_fR_{fx} + \lambda R_{fN}.$$

When the MWC rolls without slipping on the ground, R_{fx} and R_{rx} can be expressed by the next equation, where the first part concerns the rolling resistance and the second part concerns the angular momentum variation:

$$R_{fx} = -\frac{\lambda_f}{r_f}R_{fN} - \frac{I_f}{r_f^2}\gamma_G, \qquad (A3)$$

$$R_{rx} = -\frac{\lambda_r}{r_r}R_{rN} - \frac{I_r}{r_r^2}\gamma_G, \qquad (A4)$$

where λ_f and λ_r are the front and rear wheels' RP; r_f and r_r are the front and rear wheels' radii and I_f and I_r are the moment of inertia along z-dimension of the two front wheels and the two rear wheels, respectively.

Using the last two Equations (A3 and A4) in Equation (A1) then gathering the terms in γ_G allows linking the normal ground reaction forces to the COM acceleration of the loaded MWC:

$$-\frac{\lambda_f}{r_f}R_{fN} - \frac{\lambda_r}{r_r}R_{rN} = \left(m + \frac{I_f}{r_f^2} + \frac{I_r}{r_r^2}\right)\gamma_G. \qquad (A5)$$

Then, replacing R_{rN} from Equation (A2) in Equation (A5) allows expressing R_{fN}:

$$R_{fN} = -\frac{\lambda_r}{r_r}\left(\frac{r_fr_r}{\lambda_rr_f - \lambda_fr_r}\right)W + \left(m + \frac{I_f}{r_f^2} + \frac{I_r}{r_r^2}\right)$$

$$\times \left(\frac{r_fr_r}{\lambda_rr_f - \lambda_fr_r}\right)\gamma_G. \qquad (A6)$$

In the second time, the sum of the torques acting on the loaded MWC and expressed at the COM is equal to the resulting dynamic momentum, which is drastically simplified with a MWC loaded with additional masses. So, following the transversal direction:

$$(d_f + \lambda_f)R_{fN} + (-d_r + \lambda_r)R_{rN} + h(R_{fx} + R_{rx})$$

$$= -\left(\frac{I_1}{r_1} + \frac{I_2}{r_2}\right)\gamma_G, \qquad (A7)$$

where d_f and d_r are the distance between the COM and the front and rear wheels centres, respectively ($d_1 + d_2$ is the wheelbase w_b), and h is the height of the COM with respect to the ground. Then, using Equations (A1) and (A2) in A7 gives

$$\left(m + \frac{I_f}{r_fh} + \frac{I_r}{r_rh}\right)h\gamma_G = -(w_b + \lambda_f - \lambda_r)R_{fN}$$

$$+ (-d_r + \lambda_f)W. \qquad (A8)$$

Using Equation (A6) in Equation (A8) to replace R_{fN} gives

$$\left((w_b + \lambda_f - \lambda_r)\left(m + \frac{I_f}{r_f^2} + \frac{I_r}{r_r^2}\right)\left(\frac{r_fr_r}{\lambda_rr_f - \lambda_fr_r}\right)\right.$$

$$+ \left(m + \frac{I_f}{r_fh} + \frac{I_r}{r_rh}\right)h\right)\gamma_G = \left((w_b + \lambda_f - \lambda_r)\frac{\lambda_r}{r_r}\left(\frac{r_fr_r}{\lambda_rr_f - \lambda_fr_r}\right)\right.$$

$$\left.- (d_r - \lambda_r)\right)W.$$

Then, multiplying the previous equation by $(\lambda_2r_1 - \lambda_1r_2)$ and dividing by $r_1r_2w_b$ gives

$$\left(\left(m + \frac{I_f}{r_f^2} + \frac{I_r}{r_r^2}\right)\left(1 + \frac{\lambda_f - \lambda_r}{w_b}\right)\right.$$

$$+ \left(m + \frac{I_f}{r_fh} + \frac{I_r}{r_rh}\right)\left(\frac{\lambda_r}{r_r} - \frac{\lambda_f}{r_f}\right)\frac{h}{w_b}\right)\gamma_G$$

$$= \left(\frac{\lambda_f}{r_f}\frac{d_r}{w_b} + \frac{\lambda_r}{r_r}\frac{d_f}{w_b} + \frac{\lambda_f\lambda_r}{r_fr_r}\frac{r_f - r_r}{w_b}\right)W.$$

Finally, with $W = -mg$, this equation allows expressing the COM deceleration of the loaded MWC during the deceleration phase of a coast down test (cf. Equation (1)):

Appendix B

In order to quantify the terms that can be neglected in Equation (1), the deceleration value was computed 100,000 times from

Equation (1) and the two following equations:

$$\gamma_G = -mg \frac{\left(\frac{\lambda_f}{r_f} \frac{d_r}{w_b} + \frac{\lambda_r}{r_r} \frac{d_f}{w_b} \right)}{\left(m + \frac{I_f}{r_f^2} + \frac{I_r}{r_r^2} \right)}, \tag{B1}$$

$$\gamma_G = -g \left(\frac{\lambda_f}{r_f} \frac{d_r}{w_b} + \frac{\lambda_r}{r_r} \frac{d_f}{w_b} \right). \tag{B2}$$

In each step, the terms used to compute the three deceleration values were randomly chosen within their respective variation range, defined from the previous values related in the literature or from the typical values measured on MWC: the RP ranged from 1 to 3 mm (Sauret et al. 2006, 2010; Cabelguen 2008); the radii of the front wheels ranged from 30 to 100 mm and those of the rear wheels ranged from 260 to 330 mm; the radii of the wheelbase ranged between 300 and 450 mm; the COM height of the loaded MWC ranged from 500 to 700 mm; the total mass ranged between 75 and 100 kg (Coutts 1991); the moments of inertia ranged between 0.005 and 0.02 kg m^2 for the front wheels and between 0.1 and 0.2 kg m^2 for the rear wheels (Coutts 1991; Sauret 2010) and the fore-and-aft mass distribution ranged between 30% and 60% of the mass distributed on the front wheels.

The decelerations computed from Equations (1), (B1) and (B2) were then compared.

The results showed around 3.5% error comparing the accelerations computed using Equation (1) and (B1) and around 3.3% error comparing Equation (1) with Equation (B2).